

Uncertainties of Cosmic Ray Spectra and Detectability of Antiproton in SUGRA Contributions with PAMELA

A. M. Lionetto, A. Morselli, V. Zdravkovic

INFN, Sezione di Roma II, via della Ricerca Scientifica, Roma, Italy and Dipartimento di Fisica, Università di Roma "Tor Vergata", via della Ricerca Scientifica, Roma, Italy

Abstract. We studied the variation of e^+ and p top of the atmosphere spectra due to the parameters uncertainties of the Milky Way geometry, propagation models and cross sections. We used the B/C data and Galprop code for the propagation analysis. We also derived the uncertainty bands for subFe/Fe ratio, H and He. Finally, we considered a neutralino induced component in the antiproton flux in the mSUGRA framework. PAMELA expectations for positrons and antiprotons are calculated. We studied in details the possibility of disentanglement of an eventual signal component in the antiproton spectra in a clumpy halo scenario: minimal values of clumpiness factors necessary to disentangle the signal from the background without violating the quality of the antiproton data are found. There are also given examples of total spectra in comparison with existing experimental data and an example of PAMELA prediction for the total spectra. The main result of this work is that for the diffusion and convection background model PAMELA will be able to disentangle an eventual supersymmetric signal even for small clumpiness factors.

PACS numbers: 98.70.Sa; 95.35.+d; 11.30.Pb

E-mail: andrea.lionetto@roma2.infn.it, aldo.morselli@roma2.infn.it, vladimir.zdravkovic@roma2.infn.it

1. Introduction

The scope of this article is two-folded: the first part of it is dedicated to the analysis of the propagation uncertainties of cosmic rays in the Milky Way; in the second part we studied the detection possibilities of an eventual neutralino induced component in the antiproton spectra in the framework of minimal supergravity (in SUGRA).

In order to disentangle an exotic contribution from the standard one in the antiproton spectra first we have to test the accuracy of the standard calculation.

In the rest of the Introduction we give a brief description of standard mechanisms for the propagation of cosmic rays (background contribution).

In Section 2 we present the results about the uncertainties of standard propagation due to the unknown geometrical and hydrodynamic parameters of the Galaxy, uncertainties in measurements and parameterizations of nuclear cross sections and uncertainty of the helium to hydrogen ratio in the Galaxy.

In Section 3 we describe creation and propagation of a neutralino induced component (signal contribution).

In Section 4 we present PAMELA upcoming experiment expectations for theoretically predicted spectra from previous chapters.

In Section 5 we present the results about the possibility to disentangle an eventual signal component in the antiproton spectra. We did this analysis in a clumpy halo scenario, and what was found namely are minimal values of clumpiness factors necessary to disentangle the signal from the background without violating the quality of fit of the data for antiproton spectra. There are also given some examples of total spectra in comparison with the experimental data.

Section 6 contains the results and the conclusions. One of the most important conclusions of this work is that for the diffusion and convection background model, PAMELA will be able to disentangle the eventual supersymmetric signals even for small clumpiness factors.

1.1. Propagation Equation and Solar Modulation

The most complete equation for the propagation of cosmic rays that includes all the known physical processes is

$$\frac{\partial \langle r; p; t \rangle}{\partial t} = q(r; p) + r \left(D_{xx} r - V_c \right) + \frac{d}{dp} p^2 D_{pp} \frac{d}{dp} \frac{1}{p^2} \frac{\partial}{\partial p} \frac{h}{p} \frac{p}{3} (r - V_c)^i \frac{1}{f} \frac{1}{r}; \quad (1)$$

where $\langle r; p; t \rangle$ is the total phase space density. We will shortly review here the main features of the physical processes described by this equation implemented in the Galprop code [8, 13, 15, 16].

The second term describes isotropic diffusion, defined by the coefficient that depends from the rigidity (momentum per unit of charge, $r = p/Z$)

$$D_{xx} = D_0 (r = 0); \quad (2)$$

inspired by the Kolmogorov spectrum ($i = 1/3$) of the weak magnetohydrodynamic turbulence. In [14] was first shown that the Kolmogorov spectrum best reproduces

the sharp peak in B/C data. In some models we used a break in the index at some reference rigidity $\beta_1 = 0$ below β_0 while $\beta_2 > 0$ above β_0 .

The convection velocity field V_c , that corresponds to the Galactic wind, has a cylindrical symmetry. Its z-component is the only one different from zero. It increases linearly with the distance z from the Galactic plane. This is in agreement with magnetohydrodynamic models [11]. In the Galactic plane there should be no discontinuity of the convection velocity and so we considered only $V_c(z = 0) = 0$.

Reacceleration is determined by the diffusion coefficient for the impulse space D_{pp} . D_{pp} is a function of the corresponding configuration space diffusion coefficient D_{xx} and of the Alfvén velocity V_A in the framework of quasi-linear MHD theory [9, 10, 7]

$$D_{pp}(D_{xx}; V_A) = \frac{4p^2 V_A^2}{3(4 - \frac{1}{w})(4 - \frac{1}{w})w}; \quad (3)$$

where w characterizes the level of turbulence, and is equal to the ratio of MHD wave energy density to magnetic field energy density. It is assumed $w = 1$, but in any case only the quantity $V_A^2 = w$ is relevant.

The Alfvén velocity and the convection velocity gradient in Milky Way, for reacceleration and convection terms, are unknown propagation parameters (they can be determined only from the spectra of cosmic rays) and their possible range will be constrained by the analysis of sets of suitable data. The same procedure is valid for constraining the height of the galactic halo and some of the other unknown parameters. This will be analyzed further in order to obtain all the possible spectra of antiprotons and positrons using the sets of the constrained parameters. This procedure was already used in [33, 34, 35] for another propagation code, even for the antiprotons from neutralino annihilations. Among the same references can be found also a review of the propagation models in the Galaxy with an extended collection of historical and recent references.

Injected spectra of all primary nuclei are power laws in impulse

$$dq(p) = dp / p; \quad (4)$$

where the value of q can, in principle, vary with species. This power law approximation as well as a small break in the injection indexes is shown to be allowed in the framework of diffusive shock acceleration models [12, 17, 18].

Source term $q(r; p)$ for secondaries contains cross sections for their production from progenitors on H and He targets

$$q(r; p) = c_p(r; p) [\frac{ps}{H}(p)n_H(r) + \frac{ps}{He}(p)n_{He}(r)]; \quad (5)$$

where $\frac{ps}{H}(p)$ and $\frac{ps}{He}(p)$ are the production cross sections for the secondary from the progenitor on H and He targets, c_p is the progenitor density, and n_H , n_{He} are the interstellar hydrogen and helium number densities.

The last two terms in equation (1) are loss terms with characteristic times for fragmentation and radioactive decay.

The heliospheric modulation of the local interstellar spectra in the vicinity of the Earth and in the heliosphere hole has to be taken into account in order to obtain the realistic cosmic rays spectra in locations where they are/will be measured (balloon-borne or satellite-borne experiments).

We made use of a widely used and tested model in which the transport equation is solved in the force field approximation [19, 20]. That equation describes diffusion processes in the heliosphere and includes effects of heliospheric magnetic field and

solar wind. In this case, solar modulation is a function of just a single parameter that describes the strength of the modulation. All the dynamical processes are simulated simply changing the interstellar spectra during the propagation inside the heliosphere:

$$\frac{E_{\text{is}}^{\text{toa}}(E_{\text{is}}^{\text{toa}})}{E_{\text{is}}^{\text{is}}(E_{\text{is}}^{\text{is}})} = \left(\frac{p_{\text{is}}^{\text{toa}}}{p_{\text{is}}^{\text{is}}}\right)^2; \quad (6)$$

$$E_{\text{is}}^{\text{is}} \quad E_{\text{is}}^{\text{toa}} = \beta e_j; \quad (7)$$

where E and p are energies and impulses of the interstellar and top of the atmosphere fluxes and β is the unique parameter that determines the solar modulation.

2. Propagation of the Background Component of Cosmic Rays in the Milky Way and Its Uncertainties

For the treatment of the standard propagation of all the cosmic rays together we used the public Galprop code (see [8, 13, 15, 16] and references therein). We give here a short description of Galprop (based on [8], where all the details and other references can be found).

The model of the Galaxy is three dimensional with cylindrical symmetry; the coordinates are $(R; z; p)$, where R is Galactocentric radius, z is the distance from the Galactic plane, and p is the total particle momentum. The distance from the Sun to the Galactic centre is taken to be 8.5 Kpc. The propagation region is bounded fixing $R_{\text{max}} = R = 30$ Kpc and $z_{\text{max}} = z$ beyond which free escape is assumed. In Galprop, the distribution of cosmic rays sources is chosen to reproduce (after propagation) the cosmic rays distribution determined by the analysis of EGRET gamma-ray data done in [18]. The code first computes propagation of primaries, giving the primary distribution as a function of $(R; z; p)$. Then the secondary source function is obtained from the gas density and cross sections. Finally, the secondary propagation is computed.

The Galprop code includes all the processes from the propagation equation (1). Many magnetohydrodynamical parameters in the propagation equation are free and must be constrained by the cosmic ray fluxes experimental data. The second source of the cosmic ray spectra uncertainties are the uncertainties of the nuclear cross sections. These can be included by seeing how the upper and the lower propagation parameters uncertainty bounds change due to the cross section uncertainties. Some other not well known parameters like the ratio of hydrogen and helium in the Galaxy also influence the propagation. Those parameters could be estimated from other data than cosmic ray spectra.

For the final uncertainty analysis, we considered models either without reacceleration or without convection. We did not succeed in obtaining satisfactory models with all the physical processes switched on. Thus, we decided to work without both of the physical processes turned on simultaneously. A possible explanation is that one of the processes is really subdominant in the Galaxy in such a way that data require either reacceleration or convection to be well fitted. This will remain uncertain until the cosmic ray spectra are the only probe for the magnetohydrodynamics of the Galaxy, at least with the present measurements. We found the uncertainties of the two extreme cases of propagation models (see [8, 13]). In the first model are included diffusion and reacceleration effects (DR model, see previous section and equation (1)). The second model (DC) contains diffusion and convection terms from

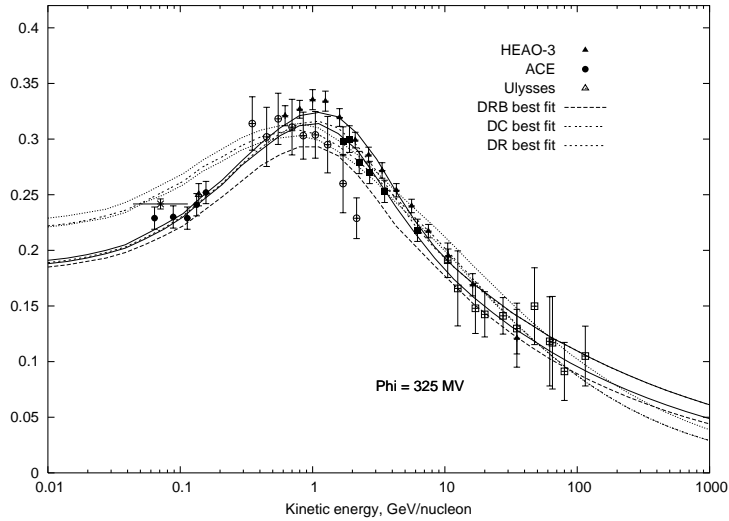


Figure 1. Propagation parameters uncertainty for B/C ratio: for DR model is given with solid lines around the best t (dashed line), while for DC model is given with dotted lines around the best t (dashed line). For DRB model we give the best t (dashed line). For the complete list of the experimental data see [50].

Table 1. Allowed values for diffusion and reacceleration model propagation parameters.

par./val.	z [K pc]	D_0 [$\text{cm}^2 \text{s}^{-1}$]			χ [K m s $^{-1}$]
minimal	3.0	$5.2 \cdot 10^{28}$	0.25	2.35	22
best t	4.0	$5.8 \cdot 10^{28}$	0.29	2.47	26
maximal	5.0	$6.7 \cdot 10^{28}$	0.36	2.52	35

the same equation (1). In this model there are two breaks: one in the index of the primary injection spectra and the other in the spectra of the diffusion coefficient D_{xx} . The first break means that at some rigidity the index suffers a discontinuity (see equation (4) and ref. [17] for details), while the second one means that at some rigidity the diffusion index suffers a discontinuity (see equation (2) and discussion in ref. [13]). For DR model we considered two sub-cases: without a break in the index of primary injection spectra and with a break at the rigidity t .

Secondary to primary CR ratios are the most sensitive quantities on variation of the propagation parameters. This can be verified numerically. Primary to primary and secondary to secondary ratios are not very sensitive to changes in the propagation parameters because they have similar propagation mechanisms. The most accurately measured secondary to primary ratio is boron to carbon ratio (B/C, see [50]). Boron is secondary while, one of its progenitors, carbon is primary. The B/C data are used also because they have relatively well known cross sections. To estimate the quality of the data we used the standard χ^2 test

$$\chi^2 = \frac{1}{N-1} \sum_n \frac{1}{(\frac{B_{\text{exp}}}{B_{\text{theo}}})^2} \left(\frac{B_{\text{exp}}}{B_{\text{theo}}} - 1 \right)^2; \quad (8)$$

Table 2. Allowed values for the propagation parameters for diffusion convection model.

par./val.	z [K pc]	D_0 [$\frac{\text{cm}^2}{\text{s}}$]	τ_2	$\frac{dV_c}{dz}$ [$\frac{\text{K m}}{\text{skpc}}$]	1	2
minimal	3.0	$2.3 \cdot 10^{28}$	0.48	5.0	2.42	2.14
best t	4.0	$2.5 \cdot 10^{28}$	0.55	6.0	2.48	2.20
maximal	5.0	$2.7 \cdot 10^{28}$	0.62	7.0	2.50	2.22

where $\tau_{\text{exp}}^{\text{B/C}}$ are statistical errors for $N = 46$ experimental points and $\tau_{\text{exp}}^{\text{B/C}}$ are measured and $\tau_{\text{teo}}^{\text{B/C}}$ are predicted values of the ratio. For the analysis of the uncertainty in the Galprop generated cosmic ray spectra induced by propagation parameters uncertainties, first we treated DR model without the break in the index of the primary injection spectra. We chose just the most important geometrical and hydromagnetic dynamical propagation parameters of this model to be varied: the height of the Galactic halo z , the constant in the diffusion coefficient D_0 (from equation (2)), the index of the diffusion coefficient (from the same equation), the primary spectra injection index for all the energies (from equation (4)) and the Alfvén velocity v_A that determines the strength of reacceleration. For the variation of the cited parameters of DR model we have required the reduced τ^2 less than 2 for the t of the B/C experimental data [50] (see figure 1). In that figure are presented the enveloping curves of all the good fits with solid lines around the best t line for the same model, that is represented with dashed line. We took the experimental data with relatively small solar modulation parameter between 325 MeV and 600 MeV, where the force field approximation is better justified than for the high modulation parameters. The allowed ranges of varied propagation parameters of this model are given in the table 1. Using the allowed parameters we found the enveloping curves of all the positron and antiproton spectra. Those enveloping curves present the upper and the lower bounds of the uncertainty bands for positron and antiproton spectra due to the propagation parameters uncertainty (see figure 2 for the positron spectra uncertainty and figure 3 for the antiproton spectra uncertainty). The relative uncertainty depends on the energy range of the spectra. For example, for positrons relative uncertainty varies from 30% under 1 GeV to 15% around 10 GeV, increasing again after 10 GeV (figure 2), while for antiprotons varies from about 10% up to about 15% (figure 3).

For a better visualization some figures that contain positron and antiproton data contain just the part of the experimental data chosen to cover in a convenient way all the energy range reached in experiments. The data are taken from references [51, 52].

In the case of DC model we chose to vary the following parameters: D_0 , the diffusion index τ_1 below the reference rigidity $\tau_0 = 4$ GV and τ_2 above it (all those parameters are from equation (2)), the halo size z , the convection velocity V_c (from equation (1)) and the injection index for primary nuclei τ_1 below the reference rigidity $\tau_0 = 20$ GV and τ_2 above it (see equation (4)). Enveloping curves of B/C fits for the reduced τ^2 values less than 2.8 are given in figure 1. Positive variations around $\tau_1 = 0$ gave unsatisfactory t . In order to take the smallest possible break of this index we decided not to take negative τ_1 values. Allowed values for the propagation parameters can be found in table 2. Again, we used them to derive the uncertainties of positron and antiproton spectra. Relative uncertainty for positrons vary between 20% above the maximum and 30% below it (figure 2) while for antiprotons is about 20% around

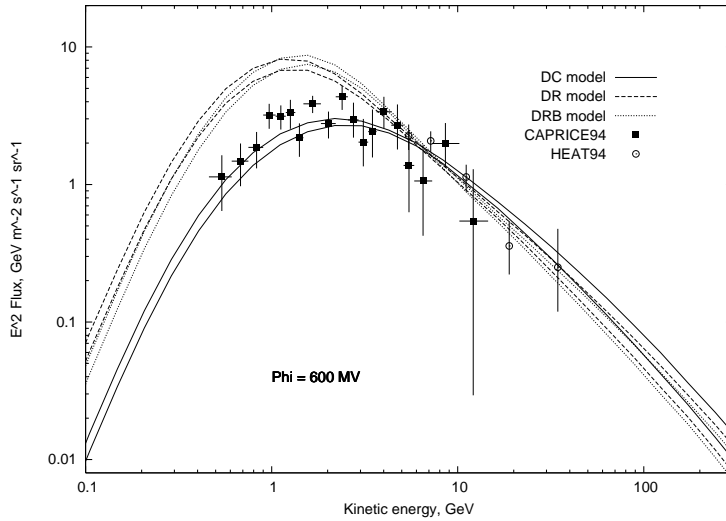


Figure 2. Upper and lower bounds of positron spectra due to the uncertainties of the propagation parameters for DC model are represented with solid lines, for DR model with dashed lines and for DRB model with dotted lines. The DR and DRB model uncertainties are very similar, but there is the slight improvement of the fit in the low energy part of the spectra in the case of DRB model. On the other side, around the maximum DRB model is overestimating the data slightly more than DR model. Experimental data are taken from [52].

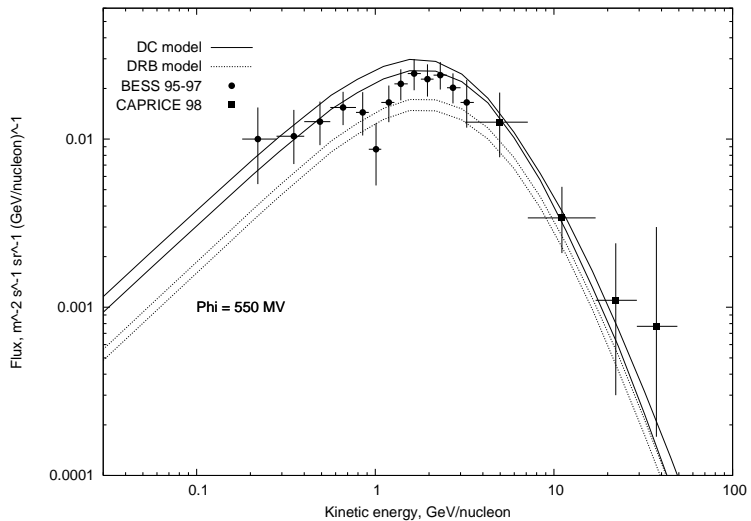


Figure 3. Upper and lower bounds of antiproton spectra due to the uncertainties of the propagation parameters for DC model (solid lines) and DRB model (dotted lines). The propagation parameters uncertainties for the DR model are almost the same as those of the DRB model (see the discussion later in the text), so we are not presenting them here to avoid the confusion. Experimental data are taken from [51].

Table 3. Allowed values for the propagation parameters for diffusion reacceleration model with break in the injection spectra of primary nuclei.

par./val.	z [K pc]	D_0 [$\frac{\text{cm}^2}{\text{s}}$]		1	2	v_A [$\frac{\text{K m}}{\text{s}}$]
minimal	3.5	$5.9 \cdot 10^{28}$	0.28	1.88	2.36	25
best t	4.0	$6.1 \cdot 10^{28}$	0.34	1.92	2.42	32
maximal	4.5	$6.3 \cdot 10^{28}$	0.36	2.02	2.50	33

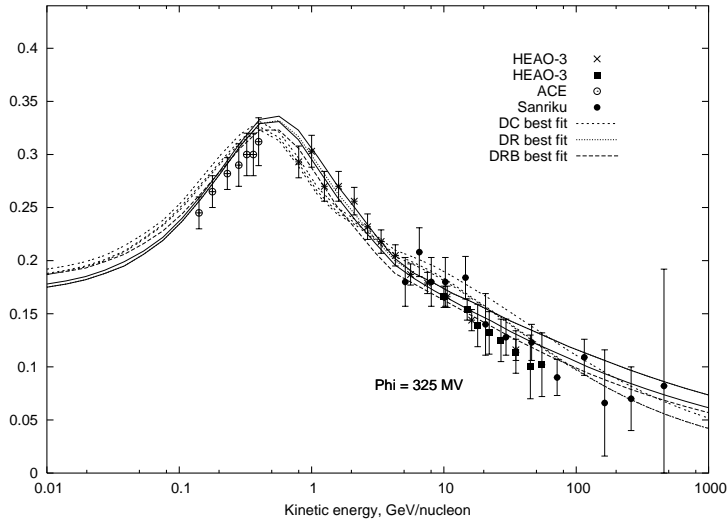


Figure 4. Ratio $(\text{Sc} + \text{Ti} + \text{V})/\text{Fe}$ that corresponds to the propagation parameters that give the best fits of B/C data for DC model is given with dashed line and it is inside the corresponding uncertainty band given with dashed lines also, for DR model is given with dotted line and it is inside the uncertainty given with solid lines, while for DRB model is given with larger-step dashed line without the uncertainty band around. Experimental data are taken from [54].

20 MeV, 17% around the maximum and 25% around 20 GeV (figure 3).

We also found the spectra that correspond to the parameters of the best fits of B/C data for subFe/Fe ratio (see figure 4), protons, helium and electrons as well as the corresponding propagation parameters uncertainties. For DC model the obtained fits are good, while DR overestimates protons (figure 7), helium (figure 6) and electrons (figure 5).

In order to improve those fits, we considered also the DR model with a break in the injection index for the primary nuclei spectra with a rigidity of 10 GV [13, 17]. We determined the allowed values of the propagation parameters (table 3) demanding the same reduced $\chi^2 = 2$ as for DR model (see figure 1). The positron and antiproton uncertainties are presented in figures 2 and 3. Even if positrons at low energies and protons and helium in all the energy range are fitted better (see figure 7 and figure 6), they remain overestimated. For the computation of B/C ratio, Galprop uses only one principal progenitor and compute weighted cross sections. Introducing the break in the index of the primary injection spectra in DR model give worst electron data fit (see figure 5) than in the case without the break. On the other side, the antiproton

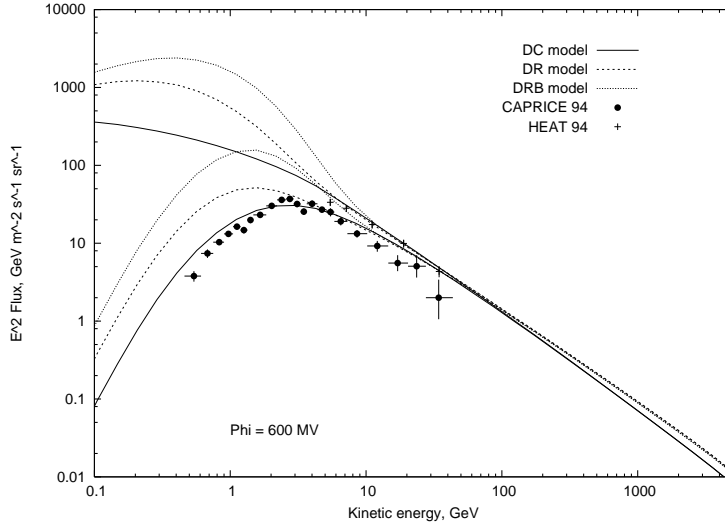


Figure 5. Top of the atmosphere spectra of electrons that correspond to the parameters of the best B/C fit are the lower curves: for DC model are given with solid line, for DR model with dashed line and for DRB model with dotted line. The local interstellar spectra are the upper curves; the three models are represented with the same types of lines. Experimental data are taken from [52].

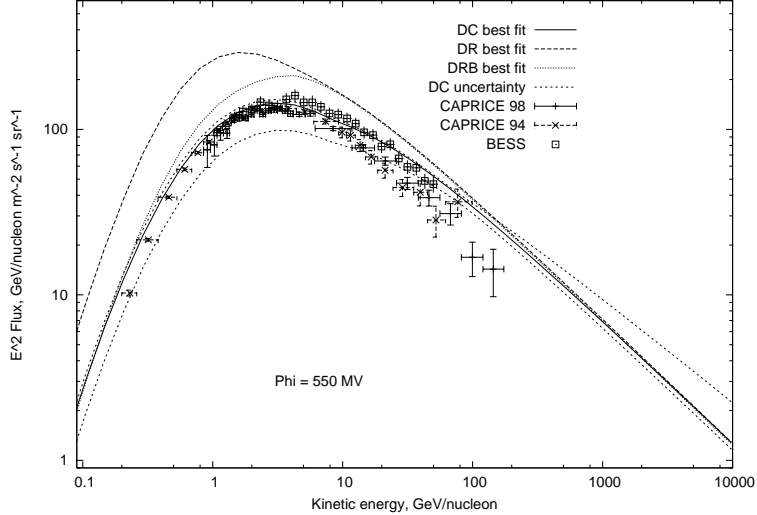


Figure 6. Upper and lower bounds of helium spectra due to the uncertainties of the propagation parameters for DC model are represented with dashed lines. Spectra that correspond to the parameters of the best B/C fit are given also for the other models: for DC model with solid line, for DR model with dashed line and for DRB model with dotted line. Experimental data are taken from [53].

spectra remain unchanged, still significantly and systematically underestimated in all the energy range.

We also calculated how the antiproton spectra change on variation of the most

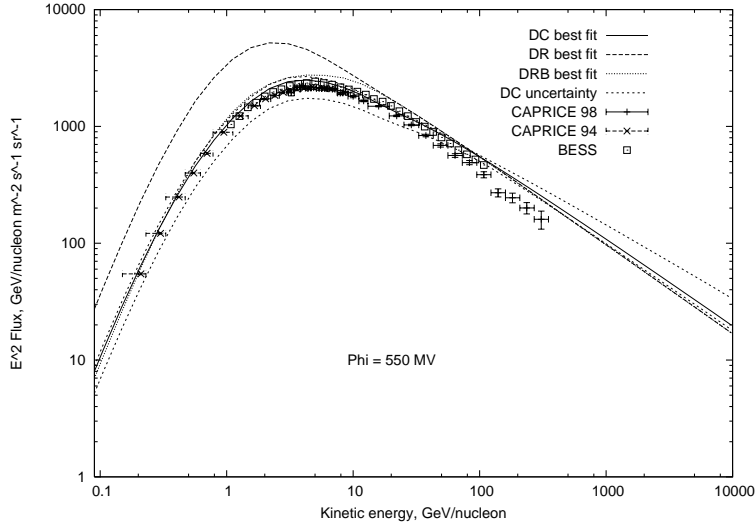


Figure 7. Upper and lower bounds of proton spectra due to the uncertainties of the propagation parameters for DC model are represented with dashed lines. Spectra that correspond to the parameters of the best B/C fit are given also for the other models. Experimental data are taken from [53].

important antiproton production cross sections. Antiprotons are created in the interactions of primary cosmic rays (protons and other nuclei) with interstellar gas. Dominant processes are interactions of high energy primary protons with hydrogen, $p + p \rightarrow p + p + p$. Parameterization of this cross section is given in [25]. Other cross sections, those of primary protons with other nuclei, are studied in reference [26]. From these, the most important are those that involve helium, and they contribute less than 20% of the total production of all the antiprotons. All the heavier nuclei together give just a few percents of the total production.

Uncertainties of cross sections influence the antiproton spectra uncertainties: simultaneous settings of all the production cross sections to the maximum/minimun rise/lower the upper/lower propagation parameters uncertainty bounds (already found before). Errors obtained in this way give contributions to the total uncertainties: they vary from 20% up to 25% in the case of DR model and, very similarly, from 20% up to 24% for DC model (depending on the energy range of the spectra). Non-production cross sections, the so called tertiary component, correspond to inelastically scattered secondaries $p + X \rightarrow p + X'$. Those processes bring down the energies of the antiprotons of relatively high energies, flattening like that the spectra. But, even if the uncertainty related to those cross sections is relatively big, this does not give relevant change of the antiproton spectra because tertiary contribution is very small. In fact, it has been implemented in propagation codes just recently.

The uncertainty in the measurements of helium to hydrogen ratio bring another component to the total uncertainty of the cosmic rays spectra. By changing the He/H ratio in a reasonable range from 0.08 to 0.11 (see [55] and [56]) we obtained a relatively small contribution. For both positron and antiproton flux uncertainty and for all of the models we considered it varies from 3% to 7%, depending on energy.

Total uncertainties of positrons and antiprotons are presented in figure 8 and in

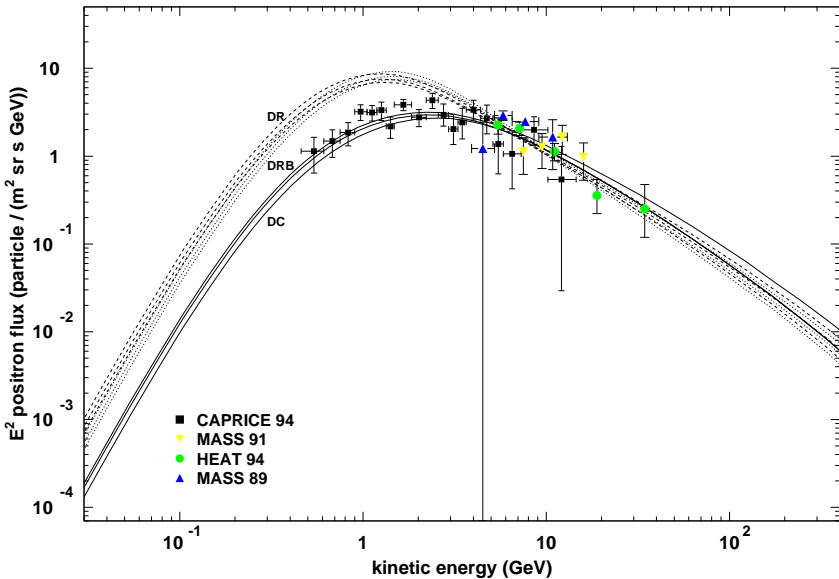


Figure 8. Total uncertainties of positron fluxes and spectra that correspond to the parameters of the best B/C fit for DC model (solid lines around the best fit curve, also solid), DR model (dashed lines around the best fit curve, also dashed) and DRB model (dotted lines around the best fit curve, also dotted). Experimental data are taken from [52]

Figure 9 respectively. They vary from 35% up to 55% for antiprotons and from 20% up to 40% for positrons for both the models in the current experimental data energy range.

In plot 10 we presented two different uncertainties of the positron spectra due to the solar modulation for the same DRB model (that fits better the data than DR model). The first uncertainty is obtained solar-modulating the lower bound of the propagation uncertainty band using the 10% bigger than measured one and the upper bound with 10% lower modulation parameter. This is a conservative error for the solar modulation parameter. The spectra are still completely above the data. As we used the force field approximation for the solar modulation, we tried also to change the modulation parameter for 50%. The resulting curves are represented on the plot and are still completely above the data. As we deal with a medium solar modulation (600MV) for positron data (we are not near the solar minimum) the sign-charge drift effect due to the solar magnetic field polarity should be not very strong.

3. Component of the Antiproton Spectra Induced by Neutralino Annihilations

In this section we take into account the possibility of a neutralino induced component in the flux. Our analysis is performed in the well known in SUGRA framework [30] with the usual gaugino mass universality at the grand unification scale M_{GUT} .

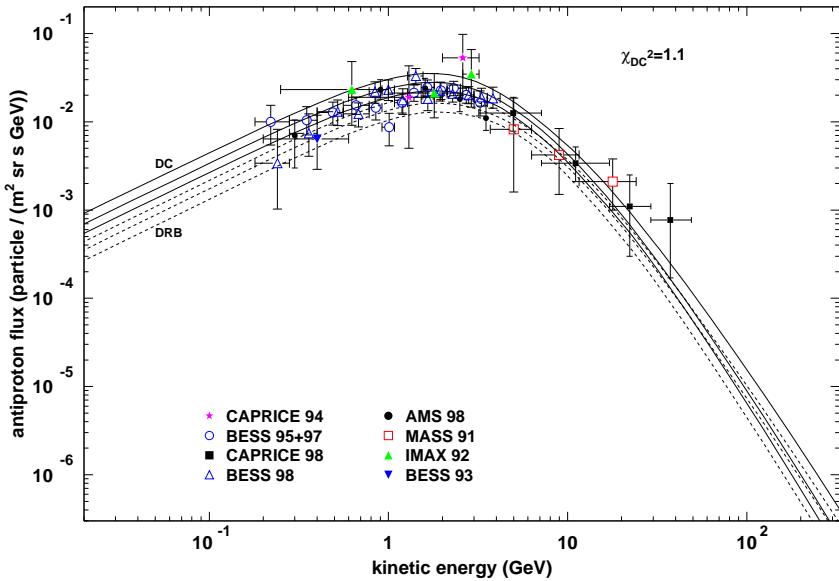


Figure 9. Total uncertainties of antiproton fluxes and spectra that correspond to the parameters of the best B/C fit for DC (solid lines around the best fit curve, also solid) and DRB model (dotted lines around the best fit curve, also dotted). Experimental data are taken from [51].

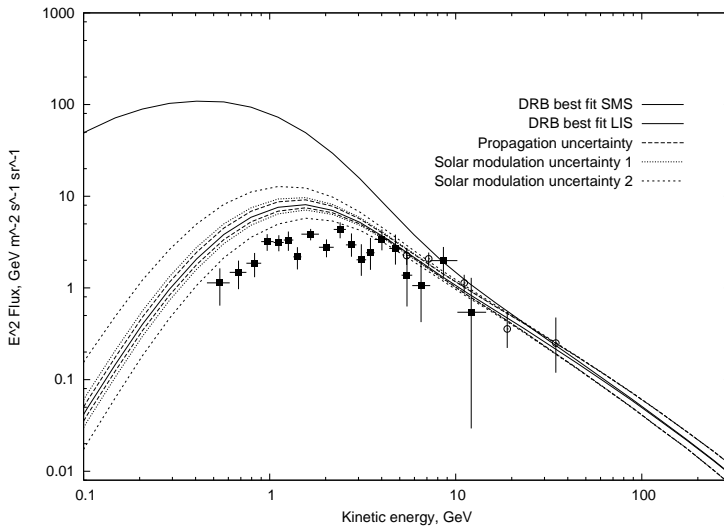


Figure 10. Top of the atmosphere (lower solid curve) and local interstellar (upper solid curve) spectra of positrons that correspond to the parameters of the best B/C fit for DRB model. Total uncertainties of positron fluxes are presented with dashed lines around the best fit. Two enlargements of the propagation uncertainties due to two different solar modulation uncertainties are presented with dotted and dashed lines (see the text for details). Experimental data are taken from [52].

In the general framework of the minimal supersymmetric extension of the Standard Model (MSSM), the lightest neutralino is the lightest mass eigenstate obtained from the superposition of four interaction eigenstates, the supersymmetric partners of the neutral gauge bosons (the bino and the wino) and Higgs bosons (two Higgsinos). Its mass, composition and couplings with Standard Model particles and other superpartners are functions of several free parameters one needs to introduce to define such supersymmetric extension. In the mSUGRA model, universality at the grand unification scale is imposed. With this assumption the number of free parameters is limited to five

$$m_{1=2}, m_0, \text{sign}(\tan\beta), A_0 \text{ and } \tan\beta;$$

where m_0 is the common scalar mass, $m_{1=2}$ is the common gaugino mass and A_0 is the proportionality factor between the supersymmetry breaking trilinear couplings and the Yukawa couplings. $\tan\beta$ denotes the ratio of the VEVs of the two neutral components of the SU(2) Higgs doublet, while the Higgs mixing α is determined (up to a sign) by imposing the Electro-Weak Symmetry Breaking (EW SB) conditions at the weak scale. In this context the MSSM can be regarded as an effective low energy theory. The parameters at the weak energy scale are determined by the evolution of those at the unification scale, according to the renormalization group equations (RGEs) [32].

For this purpose, we have made use of the ISA SUGRA RGE package in the ISA JET 7.64 software [36]. After fixing the five mSUGRA parameters at the unification scale, we extract from the ISA SUGRA output the weak-scale supersymmetric mass spectrum and the relative mixings. Cases in which the lightest neutralino is not the lightest supersymmetric particle or there is no radiative EW SB are disregarded.

The ISA SUGRA output is then used as an input in the DarkSUSY package [27]. The latter is exploited to:

reject models which violate limits recommended by the Particle Data Group 2002 (PDG) [58];

compute the neutralino relic abundance, with full numerical solution of the density evolution equation including resonances, threshold effects and all possible coannihilation processes [28];

compute the neutralino annihilation rate at zero temperature in all kinematically allowed tree-level final states (including fermions, gauge bosons and Higgs bosons);

DarkSUSY estimates the induced antiproton yield by linking to the results of the simulations performed with the Lund Monte Carlo program Pythia [57].

This setup as well as some other similar scenarios were already considered in the context of dark matter detection and of an improvement of the cosmic rays data (a list of references includes, for example, [44, 45, 46, 47, 48, 49, 29, 42, 43, 41]). The comparison of our results with previous works and other complementary techniques should be transparent.

3.1. Clumpy Halo Models

In order to obtain a higher antiproton flux in the case of high neutralino masses we assumed a small clump scenario [37] for the dark matter halo in our Galaxy. In fact,

in equation (10) the dependence of the antiproton flux is $\propto m^2$: without increasing the total halo mass by increasing the average density, there can be assumed a local density enhancement, that will also lead to the increasing of the antiproton flux.

By hypothesis the clump is a spherical symmetric compact object with mass M_{cl} and some density profile $\rho_{cl}(r_{cl})$. We denote with f the dark matter fraction concentrated in clumps and we introduce the dimensionless parameter d

$$d = \frac{1}{0} \frac{\int_0^R d^3 r_{cl} [\rho_{cl}(r_{cl})]^2}{\int_0^R d^3 r_{cl} \rho_{cl}(r_{cl})} \quad (9)$$

that gives the overdensity due to a clump with respect to the local halo density $\rho_0 = \rho(r_0)$, where r_0 is our distance from the Galactic Center (GC). In a smooth halo scenario the total neutralino induced flux calculated for $r = r_0$ is given by [38]

$$f_p(r_0; T) = \frac{\chi_{\text{ann}} v}{f} \frac{dN^f}{dT} B^f \frac{m_0}{m} C_{\text{prop}}(T) : \quad (10)$$

where T is the particle kinetic energy, $\chi_{\text{ann}} v$ is the total annihilation cross section times the relative velocity, m is the neutralino mass, B^f and $dN^f = dT$, respectively, the branching ratio and the number of p produced in each annihilation channel f per unit energy and $C_{\text{prop}}(T)$ is a function entirely determined by the propagation model. In the presence of many small clumps the flux is given by

$$f_p^{\text{clump}}(r_0; T) = f d f_p(r_0; T) \quad (11)$$

For the smooth profile we assumed a Navarro, Frenck and White profile (NFW) [39].

3.2. Propagation of the Neutralino Induced Component

The primary contribution to the antiproton flux is computed using the public code DarkSUSY [40]. We modified the antiproton propagation in order to be consistent with the DC propagation model as implemented in Galprop code. We assumed diffusion coefficient spectra used in Galprop code with our best fit values for the diffusion constants D_0 and D_1 . In DarkSUSY, the convection velocity field is constant in the upper and the lower Galactic hemispheres (with opposite signs, and so it suffers unnatural discontinuity in the Galactic plane), while Galprop uses magnetohydrodynamically induced model, in which one component of velocity field along the Galactic latitude (the only one that is different from zero) increases linearly with the Galactic latitude [11]. We assumed an averaged convection velocity calculated from the Galactic plane up to the Galactic halo height z .

4. Detection of the Secondary Components in the Positron and the Antiproton Fluxes by PAMELA

In this section we calculate the statistical errors for the PAMELA [22, 24] experiment for the positron and the antiproton background spectra calculated with Galprop z .

The calculation is done for a three years mission assuming the geometric factor given in figure 11 taken from the results of the test measurements on triggers with the first and the last scintillators of the apparatus [23]. PAMELA's statistical errors for positrons and antiprotons in the case of the DC model are given in figure 12 and in

^z The list of the people and the institutions involved in the collaboration together with the on-line status of the project is available at <http://wizard.roma2.infn.it/>.

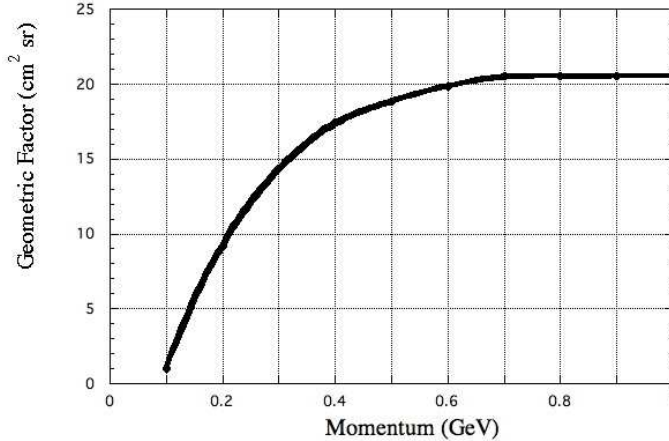


Figure 11. Geometric factor of PAMELA

Figure 13. For the antiprotons we also present the expectations for DRB propagation model in the figure 14 for completeness. We do not present PAMELA's expectations for antiprotons in the DR model case because the DR model flux that correspond to the best B/C ratio propagation parameters is almost identical with that of DRB model. DR and DRB model background PAMELA predictions for positron fluxes are not given because those fluxes largely overestimate the experimental data at low energies.

5. The Possibility of Disentanglement of the Neutralino Induced Component in the Antiproton Flux With PAMELA

In this section we present the results we found about the minimal values of the clumpiness factors f_d needed to disentangle a neutralino induced component in the antiproton flux with PAMELA. We computed this factor as a function of the SUGRA parameters, fixing A_0 , $\tan\beta$ and $\text{sign}(\mu) = 1$. In this way the clumpiness factor becomes a function of m_0 and $m_{1=2}$ parameters. Similar analysis were already made in the literature (see for example [29, 42, 43, 41]).

For the discrimination we requested the following conditions:

- (i) The total antiproton flux $\text{tot} = \text{bkg} + \text{susy}$ gives a good fit of the experimental data.
- (ii) Difference between tot and DC model bkg is detectable by PAMELA.

The first condition is satisfied if

$$\chi^2_{\text{fit}} = \frac{1}{N-1} \sum_{n=1}^N \frac{(\frac{\text{exp}}{m} - \frac{\text{tot}}{m})^2}{(\frac{\text{exp}}{m})^2} \quad (12)$$

is less than the $\chi^2_{\text{fit},0} = 1.7$, for $N = 40$ experimental points. The second condition is satisfied if

$$\chi^2_{\text{discr}} = \frac{1}{M-1} \sum_{m=1}^M \frac{(\frac{\text{bkg}}{m} - \frac{\text{tot}}{m})^2}{(\frac{\text{Pbkg}}{m})^2} \quad (13)$$

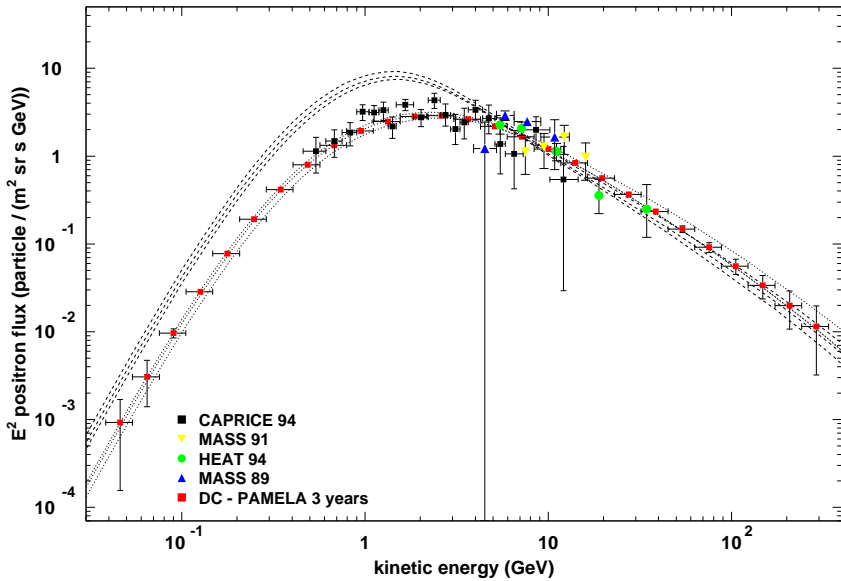


Figure 12. Experimental data (from [52]) confronted with PAMELA's expectations for positrons for DC model background. Total uncertainties of positron fluxes with the spectra that correspond to the parameters of the best B/C fit in the middle are given for better confrontation: for DC model they are represented with dotted lines while for DRB model with dashed lines.

is greater than the $\chi^2_{\text{discr},0} = 1.8$, for $M = 29$ points, where χ^2_{bkg} are the PAMELA statistical errors associated to the background flux (those presented in figure 13).

The reduced χ^2_{fit} for the background flux alone is $\chi^2_{\text{fit}} = 1.1$. This means that the background already gives a good fit of the experimental data.

5.1. Results

For each model we found the minimal value of the clumpiness factor f_d needed to satisfy both conditions. As the clumpiness factor is a function of m_0 and $m_{1=2}$ parameters we made contour plots calculating equi-clumpiness factors lines. First, we found the results for different values of $\tan\beta$, presented in figure 15 and in the left panel of the figure 20. Then we examined in more details some interesting zones in those plots. The regions in parameter space that are excluded either by accelerator bounds or because electroweak symmetry breaking is not achieved or because the neutralino is not the lightest supersymmetric particle are represented with black color. Red (dark shaded) color indicates the $(m_0, m_{1=2})$ domains with h^2 in the WMAP [1] region $0.09 < h^2 < 0.13$. Green (light shaded) color indicates the parameter space regions with values of $0.13 < h^2 < 0.3$. Equi-clumpiness factors lines are given with black solid lines. Beside every line it is indicated the value of the clumpiness factor. Under the line $f_d = 1$ there are no models that satisfy at the same time the both conditions from equations (12) and (13).

As an example we give in the right panel of figure 17 a plot with that region

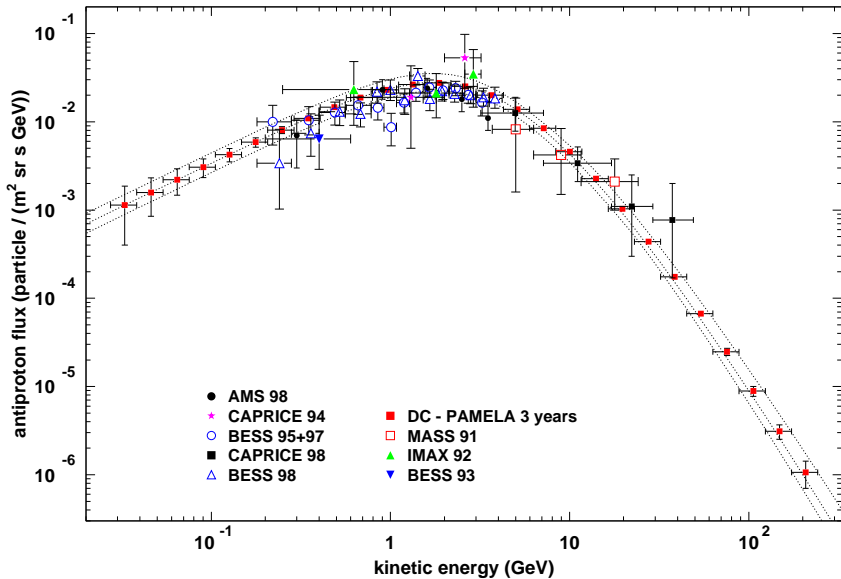


Figure 13. Experimental data (from [51]) confronted with PAMELA's expectations for antiprotons for DC model background. Total uncertainty of the DC model antiproton background flux with the spectra that correspond to the parameters of the best B/C fit in the middle are given for better confrontation; they are represented with dotted lines. The reduced χ^2 is 1.1 that means that the background gives a very good fit.

colored in blue. For the reader benefit we also give in figure 16 and in the right panel of figure 20 the equineutralino mass contours for different values of $\tan\beta$. It can be seen that even small clumpiness factors (of order 10) are sufficient for PAMELA detection. This is very important, because, even if we consider a DC model as the background flux (that alone already gives a good fit of the experimental data) it is still possible to disentangle a supersymmetric component in a wide region of the parameter space (in comparison with the WMAP allowed zone). The two favourite cases are: $\tan\beta = 55$ (see figure 15) and $\tan\beta = 60$ (see figure 20).

In figure 17 we presented one of the two particularly interesting regions, namely those inside the cosmologically allowed zone, found for the $\tan\beta = 50$ case, i.e. that from the left panel of figure 15. The other interesting region, corresponding to the so called focus point region [...] in which the neutralino has a significant higgsino component, is presented in figure 18. We can see that for those cases the region in the parameter space that corresponds to both conditions satisfied, (12) and (13), and that gives the right relic density h^2 , is not very big with respect to the total cosmologically allowed zone. The red zone mainly corresponds to small clumpiness factors, i.e. less than 20.

In the $\tan\beta = 55$ case (see the right panel of figure 15) there is the maximally extended cosmologically allowed region, and a huge part of it lies between the equicloudiness factors lines $fd = 1$ and $fd = 10$. So, the disentanglement of the

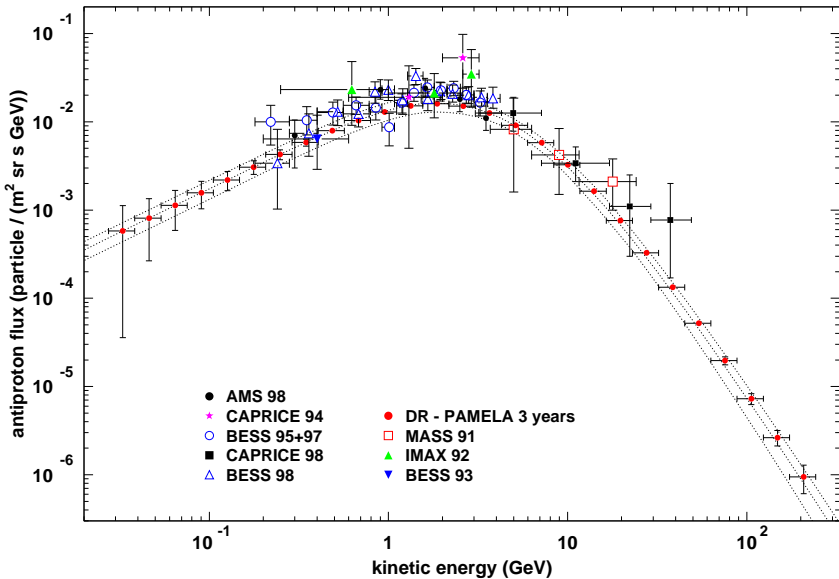


Figure 14. Experimental data (from [51]) confronted with PAMELA's expectations for antiprotons for DRB model background. Total uncertainty of the DRB model antiproton background flux with the spectra that correspond to the parameters of the best B/C fit in the middle are given for better confrontation; they are represented with dotted lines.

supersymmetric signal is achieved without increasing the minimal clumpiness factors.

In figure 19 we gave two three dimensional graphics that represent the functional dependence of the fd factor from m_0 and m_{1-2} : the left panel corresponds to figure 17 while the right one corresponds to the right panel of the figure 15.

The last case is that of $\tan\beta = 60$ (see figure 20) in which one red zone is completely between the lines with $fd = 1$ and $fd = 10$.

5.2. Some Examples of the Primary Component of the Antiproton Flux

In this section we present four different contributions to the antiproton flux induced by neutralino annihilations. Fluxes are calculated for different neutralino masses obtained from particular choices of the various SUGRA parameters that satisfy the WMAP limits on the cosmological relic density and for different choices of the clumpiness factors fd .

Higher neutralino masses produce primary contributions that improve high energy data fits but with a need of high clumpiness factors, due the dependence from the inverse neutralino mass squared m^{-2} in the primary antiproton flux formula (10).

Small neutralino masses produce relatively high fluxes at small energies where the data are already fitted with a background contribution only. As a consequence a relatively small part of the various SUGRA parameter space gives the primary contributions that satisfies the experimental data fit.

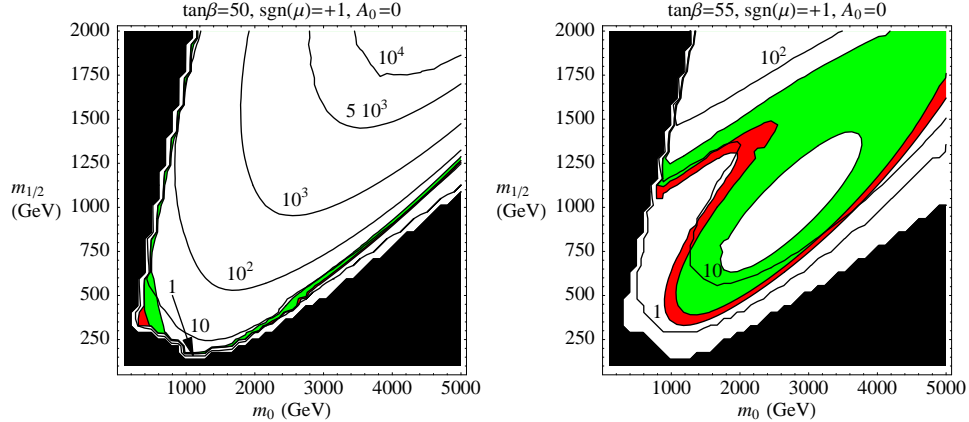


Figure 15. Equi-clumpiness factors lines as functions of m_0 and $m_{1/2}$ parameters. In the left panel $\tan\beta = 50$ while in the right panel $\tan\beta = 55$. The other parameters are $A_0 = 0$ and $\text{sgn}(\mu) = +1$. Black color represents the regions in the parameter space that are excluded either by accelerator bounds or because electroweak symmetry breaking is not achieved or because the neutralino is not the lightest supersymmetric particle. Red (dark shaded) are domains with h^2 in the WMAP region $0.09 < h^2 < 0.13$, while green (light shaded) are the parameter space domains with $0.13 < h^2 < 0.3$. Under the line with $fd = 1$ there are no models that satisfy the both conditions (12) and (13).

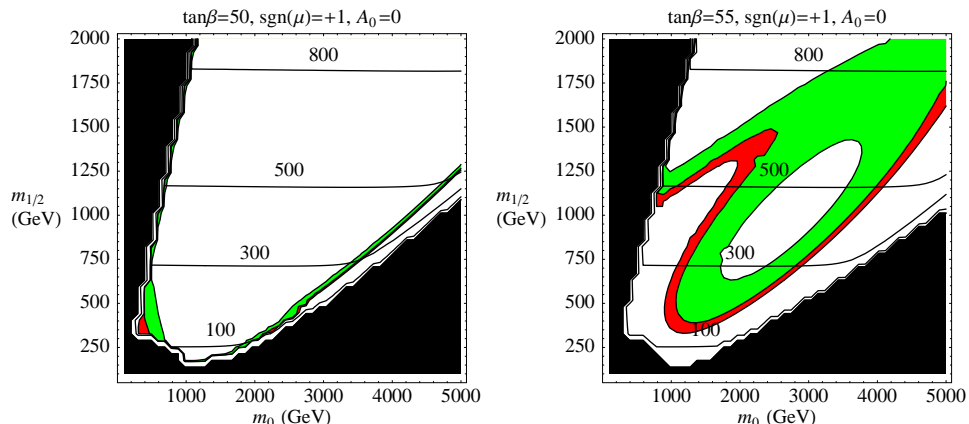


Figure 16. Equineutralino mass (expressed in GeV) lines as functions of m_0 and $m_{1/2}$ parameters. In the left panel $\tan\beta = 50$ while in the right panel $\tan\beta = 55$. The other parameters are $A_0 = 0$ and $\text{sgn}(\mu) = +1$. Black color represents the regions in the parameter space that are excluded either by accelerator bounds or because electroweak symmetry breaking is not achieved or because the neutralino is not the lightest supersymmetric particle. Red (dark shaded) are domains with h^2 in the WMAP region $0.09 < h^2 < 0.13$, while green (light shaded) are the parameter space domains with $0.13 < h^2 < 0.3$. Under the line with $fd = 1$ there are no models that satisfy the both conditions (12) and (13).

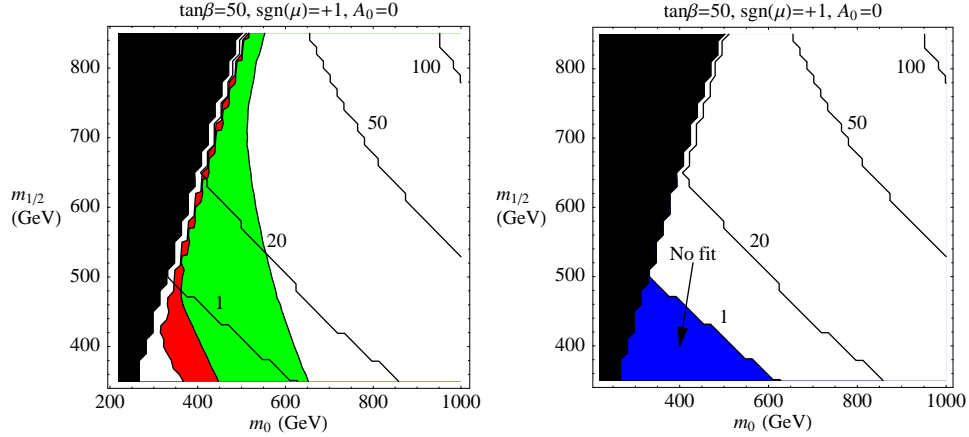


Figure 17. Left: equi-clumpiness factors lines as functions of m_0 and $m_{1/2}$ parameters in the first interesting part of the parameter space ("zoomed" on the WMAP allowed zone) for $\tan\beta = 50$. Regions in the parameter space that are excluded either by accelerator bounds or because electroweak symmetry breaking is not achieved or because the neutralino is not the lightest supersymmetric particle are black. Domains with h^2 in the WMAP region $0.09 < h^2 < 0.13$ are red, while green indicates regions with $0.13 < h^2 < 0.3$. Right: the same plot as in the left panel, but with blue region under the line with $f_d = 1$ in which there are no models that satisfy the both conditions (12) and (13) simultaneously.

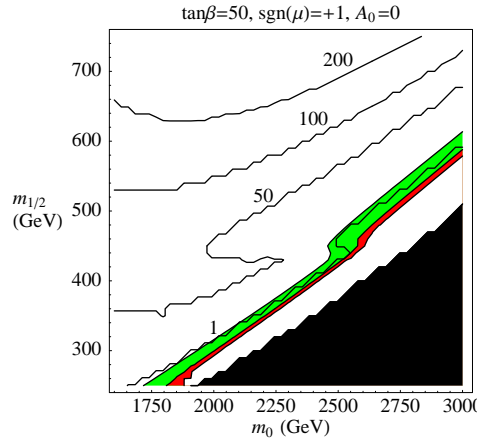


Figure 18. Equi-clumpiness factors lines as functions of the m_0 and $m_{1/2}$ parameters in the second interesting part of the parameter space ("zoomed" on the WMAP allowed zone) for $\tan\beta = 50$. Regions in the parameter space that are excluded either by accelerator bounds or because electroweak symmetry breaking is not achieved or because the neutralino is not the lightest supersymmetric particle are black. Domains with h^2 in the WMAP region $0.09 < h^2 < 0.13$ are red, while green indicates regions with $0.13 < h^2 < 0.3$.

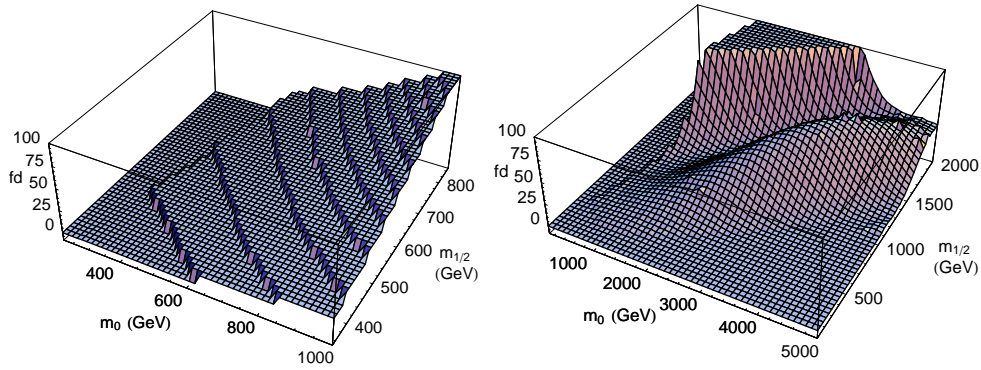


Figure 19. Clumpiness factor as a function on the $(m_0, m_{1/2})$ plane for $\tan\beta = 50$ in the "zoomed" zone from the figure 17 (left panel) and for $\tan\beta = 55$ for all the masses we considered, i.e. the whole mass zone from the right panel from the figure 15 (right panel).

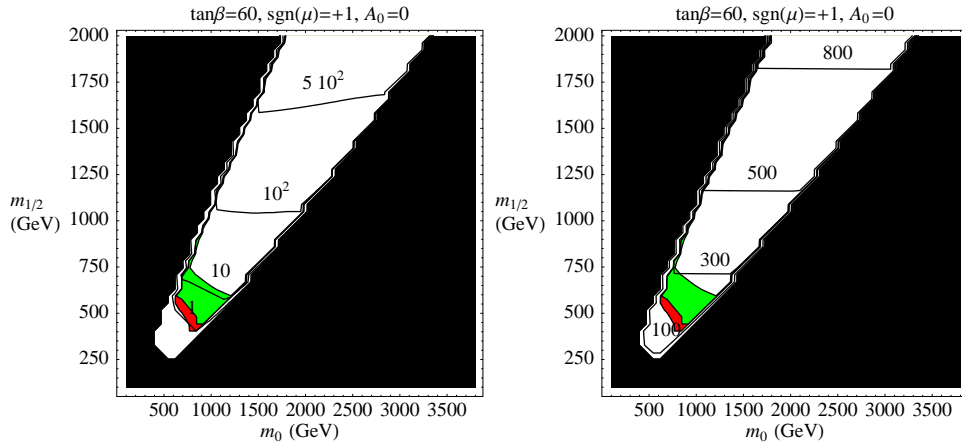


Figure 20. Left: equi-clumpiness factors lines as functions of m_0 and $m_{1/2}$ parameters for $\tan\beta = 60, A_0 = 0$ and $\text{sgn}(\mu) = +1$. Black color represents the regions in the parameter space that are excluded either by accelerator bounds or because electroweak symmetry breaking is not achieved or because the neutralino is not the lightest supersymmetric particle. Red (dark shaded) are domains with h^2 in the WMAP region $0.09 < h^2 < 0.13$, while green (light shaded) are the parameter space domains with $0.13 < h^2 < 0.3$. Under the line with $fd = 1$ there are no models that satisfy the both conditions (12) and (13) simultaneously. Right: The equineutralino mass lines with the same color coding.

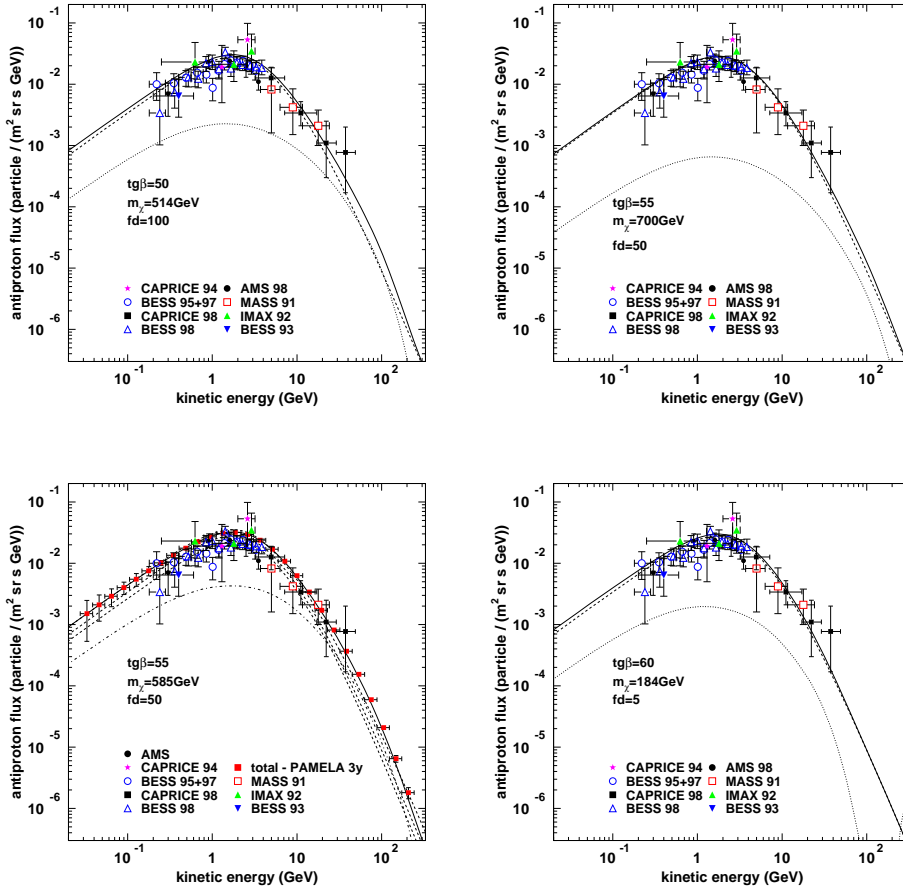


Figure 21. Different neutralino annihilations induced contributions to the total antiproton flux with the DC model background that corresponds to the propagation parameters of the best fit of the B/C data. The dashed lines correspond to the background contributions, the punctuated lines correspond to the neutralino induced contributions, while the solid lines correspond to total antiproton fluxes. As an example, for the third model we show also the PAMELA expectations for the total flux.

6. Conclusions

In the first part of this work we deduced systematically the uncertainties of the most important cosmic rays spectra, with an emphasis on positrons and antiprotons. For positrons in DR model the curve of the minimal positron production still remains above the experimental results, even when the uncertainties are included. Breaking the index of the primary spectra (DRB model) proves just the low energy part of the spectra below the maximum, but the minimal predictions still remain above the experimental results around the maximum (where due to the break now are produced slightly more positrons) as well as below it. On the other side, the attempt to improve

the DR model results slightly affects the best B/C experimental data fit. The break is also not sufficient to match protons and helium data, that are still overestimated. Electrons remain largely overproduced at low energies, even more than in the case without the break, i.e. in DR model.

For the model with diffusion and convection all the results are in excellent agreement with the data except in the B/C case. This problem could be due to some other sources of uncertainties, like the interstellar gas distribution, solar modulation and approximations done in the cross section calculations. As a possibility for future analysis we would like to emphasize that it is natural to take into account models that include both of the processes, convection and reacceleration. Perhaps, this can be a key to solve simultaneously the problem with positrons, electrons, primaries and B/C ratio.

In any case, further measurements of antiproton and positron spectra, primary to secondary CR ratios and solar effects on them, as well as the precise determination of important nuclear cross sections seem to be crucial to determine the correct propagation model.

The upper uncertainty bands of the antiproton spectra for those models that include reacceleration touch the experimental data from below. In those cases the experimental data fits can be easily improved adding different primary components coming from neutralino annihilations or from some other exotic contributions.

In the framework of the DC model, exotic contributions remain possible at high energies ($E > 20$ GeV) and not excluded at lower energies, due to the relatively large background uncertainties.

In the second part of this work, we treated the detection of cosmic rays with the upcoming PAMELA experiment with an emphasis on the antiprotons. We calculated the statistical errors associated to the detection of positron and antiproton fluxes for different propagation models. We studied in details the detection possibility of an eventual supersymmetric component in the antiproton spectra for a large domain in the parameter space of the SUGRA models. The most important conclusion is that for PAMELA disentanglement of a neutralino induced component in the antiproton spectra are sufficient a relatively small clumpiness factors, of the order $f_d / 10$. We considered a DC model flux as the background that already fits the experimental data, in contrast to DR models for the standard propagation that systematically underestimate the data and allow almost any supersymmetric contribution. In the case of the DC background, it is still possible to disentangle a supersymmetric component for a relatively large (in the comparison with the WMAP allowed zones) portion of the parameter space even for small clumpiness factors.

- [1] Bennett C L et al 2003 *Astrophys. J. Suppl.* 148 1
- Spergel D N et al 1985 *Phys. Rept.* 117 75
- [2] Dimopoulos S and Sutter D W 1995 *Nucl. Phys. B* 452 496
- [3] Gabiani F, Gabrielli E, Masiello A and Silvestrini L 1996 *Nucl. Phys. B* 477 321
- [4] Giudice G F and Masiello A 1988 *Phys. Lett. B* 206 480
- [5] Casas J A and Munoz C 1993 *Phys. Lett. B* 306 288
- [6] Dvali G R, Giudice G F and Pomarol A 1996 *Nucl. Phys. B* 478 31
- [7] Berezhinskii V S, Bulanov S V, Dوجiel V A, Ginzburg V L, Ptuskin V S 1990 *Astrophysics of Cosmic Rays* (North Holland, Amsterdam)
- [8] Strong A W and Moskalenko I V 1998 *ApJ* 509 212
- [9] Fermi E 1949 *Phys. Rev.* 75 1169
- [10] Seo E S and Ptuskin V S 1994 *ApJ* 431 705

- [11] Zirakashvili V N, Breitschwerdt D, Ptuskin V S and Volk H J 1996 *A & A* 311 113
- [12] Blandford R D and Ostriker J P 1980 *ApJ* 237 793
- [13] M oskalenko I V, Strong A W, Omes and J F Pottgieter M S 2002 *ApJ* 565 280
- [14] Heinrich U and Simon M 1995 *ApJ* 441 209-221
- [15] Strong A W and M oskalenko I V *Galprop C++ v.41: Explanatory supplement*, available on the [WWW](http://www.astro.wisc.edu/~strong/galprop/)
- [16] M oskalenko I V and Strong A W 1998 *Astrophys.J.* 493 694-707
- [17] Ellison D C et al 2001 *ApJ* 563 191-201
- [18] Strong A W and M attox J R 1996 308 L21
- [19] Gleeson L J and Axford W I 1996 *ApJ* 154 1011
- [20] Perko J S 1987 *A & A* 184 119
- [21] Bieber J W, Burger R A, Engel R, Gaisser T K, Roesler S and Stanev T 1999 *Phys. Rev. Lett.* 83 674
- [22] Adriani O et al 2002 *Nucl. Inst. and Methods in Phys. Research A* 478 114-118
- [23] Papini P 2004 private communication
- [24] Picozza P and Morselli A 2003 *J. Phys. G: Nucl. Part. Phys.* 29 903-911
- [25] Tan L C and Ng L K 1983 *J. Phys. G* 9 227
Tan L C and Ng L K 1983 *J. Phys. G* 9 1289
- [26] Gaisser T K and Schaefer R K 1992 *ApJ* 394 174
- [27] Gondolo P, Edsjo J, Ullio P, Bergstrom L, Schelke M and Baltz E A *Preprint astro-ph/0211238*
- [28] Edsjo J, Schelke M, Ullio P and Gondolo P 2003 *JCAP* 0304 001
- [29] Profumo S and Ullio P 2004 *JCAP* 0407 006
- [30] Hall L J, Lykken J, and Weinberg S 1983 *Phys. Rev. D* 27 2359
- [31] Chan K L, Chattopadhyay U, Nath P 1997 *Phys. Rev. D* 58 096004
Feng J L, Matchev K T, M oroit 2000 *Phys. Rev. Lett.* 84 2322
Feng J L, Matchev K T, M oroit 2000 *Phys. Rev. D* 61 075005
Baer H et al 2003 *J. High Energy Phys.* 0306 054
- [32] Cesarini A, Fucito F, Lionetto A, Morselli A and Ullio P 2004 *Astropart. Phys.* 21 267
- [33] Donato F et al 2001 *ApJ* 536 172
- [34] Donato F, Fomengo N, M aurin D, Salati P and Taillet R 2003 *Phys. Rev. D* 69 06350
- [35] Donato F et al 2002 *Preprint astro-ph/0212111*
- [36] Baer H, Paige F E, P rotopopescu S D and Tata X *Preprint hep-ph/0001086*
- [37] Bergstrom L, Edsjo J, Gondolo P and Ullio P 1999 *Phys. Rev. D* 59 043506
- [38] Bergstrom L, Edsjo J and Ullio P *Preprint astro-ph/9902012*
- [39] Navarro J F, Frenk C S and White S D M 1996 *ApJ* 462 563
- [40] Gondolo P, Edsjo J, Ullio P, Bergstrom L, Schelke M and Baltz E A 2004 *JCAP* 0407 008
- [41] de Boer W et al 2003 *Preprint IEKP-KA/2003-17, [hep-ph/0309029]*
- [42] Bottino A et al 2004 *Phys. Rev. D* 69 063501
- [43] Bottino A et al 1998 *Phys. Rev. D* 58 123503
- [44] Feng J L, Matchev K T and W ilczek F 2001 *Phys. Rev. D* 63 045024
- [45] Bottino A, Donato F, Fomengo N and Scopel S 2001 *Phys. Rev. D* 63 125003
- [46] Ellis J, Feng J L, Ferstl A, Matchev K T and Olive K A 2002 *Eur. Phys. J. C* 24 311-322
- [47] Ellis J, Ferstl A and Olive K A 2002 *Phys. Lett. B* 532 318
- [48] Bertin V, Nezri E and Orl o J 2002 *Eur. Phys. J. C* 26 111
- [49] Chattopadhyay U, Corsetti A and Nath P 2003 *Phys. Rev. D* 68 035005
- [50] Davis A J et al 2000 *AP Conf. 528*, ed. M ewaldtet R A al (AIP, New York)
Du Vernois M A et al 1996 *A & A* 316 555
Lukasiak A et al 1999 *Proc. 26th Int. Cosmic-Ray Conf. (Salt Lake City)* 3 41
Engelmann J J et al 1990 *A & A* 233 96
Caldwell J H and Meyer P 1977 *Proc. 15th Int. Cosmic-Ray Conf. (Plovdiv)* 1 243
Dwyer R et al 1978 *ApJ* 224 691
Juliusson E et al 1974 *ApJ* 191 331
Simon M et al 1980 *ApJ* 239 712
- [51] B oezio M et al 2001 *Astrophys. Journ.* 561 787
Orto S et al 2000 *Phys. Rev. Lett.* 84 1078
M aeno T et al 2001 *Astroparticle Physics* 16 121-128
B oezio M et al 1997 *Astrophys. Journ.* 487 415
M oiseev A et al 1997 *Astrophys. Journ.* 474 479
M itchell J W et al 1996 *Phys. Rev. Lett.* 76 3057
Basini G et al 1999 *Proc. 26th ICRC OG 1.1.21*
Guilard M et al 2002 *Phys. Rep.* 366/6 331

- [52] Bœtio M et al 2000 *ApJ* 532 653
Barwick S et al 1997 *ApJ* 498 779
Grimani C et al 2002 *A&A* 392 287-294
Golden R L 1994 *ApJ* 436 769-775
- [53] Bœtio M et al 2003 *Astroparticle Physics* 19 583-604
Bœtio M et al 1999 *ApJ* 518 457-472
Sanuki T et al 2000 *ApJ* 545 1135
- [54] Davis A J et al 2000 On the low energy decrease in Galactic cosmic ray Proc ACE-2000 Symp. ed. Mewald R A et al (NY: AIP) AIP Conf. Proc. 528 421-424
Binns W R et al 1988 *ApJ* 324 1106-1117
Engelmann J J et al 1990 *A&A* 233 96-111
Hareyama M et al 1999 26th ICRC (Salt Lake City) 3 105-108
- [55] Grevet N, Noels A and Sauval A J 1996 *ASP Conf. Ser.* 99, *Cosmic Abundances* ed. Holt S S and Sonneborn G (San Francisco: ASP) 117
- [56] Hernandez F P and Christensen-Dalsgaard J 1994 *MNRAS* 269 475
- [57] Sjøstrand T 1994 *Comput. Phys. Comm.* 82 74
- [58] Hagiwara K et al 2002 *Phys. Rev. D* 66 010001
- [59] Maurin D, Taillet R and Donato F 2002 *A&A* 394 1039